Analysis, Design, and Implementation of a New Extremely Ultrathin 2-D-Isotropic Flexible Energy Harvester Using Symmetric Patch FSS

Alireza Ghaneizadeh, Mojtaba Joodaki, *Senior Member, IEEE*, Josef Börcsök, Abbas Golmakani, and Khalil Mafinezhad, *Member, IEEE*

***Abstract*— Electromagnetic (EM) energy exists far and wide in the environment and can be harnessed and transferred to the desired load(s). The researchers mostly designed and implemented the planar metasurface energy harvester (MEH) offering a restricted look-angle. In this article, we propose an extremely ultrathin 2-D-isotropic flexible MEH using multipolarized patch frequency selective surface. This MEH, which has a curved shape, enjoys a relatively constant performance over a huge range of oblique incident waves. The final structure can be prepared by a small slice of a cylinder. A classic model inspired from the dipole antenna concept is used for impedance matching. Theoretical analyses, design, and fabrication of the structure are presented using a deep subwavelength PCB substrate having a thickness of ∼0.004 λ_0. EM energy harvesting is analyzed with an equivalent circuit model. The experimental results are acceptably in agreement with the simulation results. The design can be scaled to different RF bands; however, to provide the required energy for Internet-of-Things (IoT) instruments, we have used WiFi as a crowded frequency band. The simulation efficiency of the flat style extremely ultrathin MEH (EMEH) for normal incidence (at 5.81 GHz) and 60° oblique angle incidence with transverse magnetic (TM) and transverse electric (TE) polarizations are 87.35%, 93.26%, and 64.42%, respectively. In addition, half power bandwidth (HPBW) for these situations is 6.97%, 8.86%, and 5.61%, respectively.**

***Index Terms*— Absorber, dipole antenna, electromagnetic (EM) energy harvesting, metasurface, wireless power transfer (wpt).**

I. Introduction

INTERNET-OF-THINGS (IoT) has recently turned into one of the most discussed subjects in different communities of researchers and still its significance has yet to be covered [1]. It is known that power supply sources are the key issues to realize this concept as the communication between numerous smart sensors is required in each subsystem [1], [2]. Nevertheless, in more traditional methods, wiring and battery storage can be used as their sources; however, the abundance of sensors makes traditional methods rather impractical and cost-inefficient [1], [2]. Alternatively, electromagnetic (EM) energy harvesting is assumed to be a solution to overcome the shortcomings of traditional supplies [1], [2].

Ramahi *et al.* [3] introduced a new collector with nearly perfect power reception using metasurface concept [4], [5]. The most frequently proposed metasurface energy harvesters (MEHs) in the literature are namely grounded substrate and classified into two typical resonators (split ring and complementary split ring resonators) [6], [7]. Since 2012, many types of MEH architectures have been developed, for example, multipolarized [8]–[10], multibands [7], [11], wideband [6], [12], and wide angles [6], [7], [11] receptions. Despite this impressive progress, the majority of previous approaches have not been able to provide a flexible MEH to enhance its applicabilities. For the first time, in our work [13], an ultrathin 2-D-isotropic flexible MEH as a new classification of harvesters was designed and implemented; however, the harvester is still sensitive to the orientation of wave polarization. To the best of our knowledge, a flexible MEH insensitive to polarization has not been reported in the literature. Therefore, developing this new design of MEH is still needed to open up practical wireless powering applications with arbitrary shapes.

In this article, a new extremely ultrathin flexible MEH is analyzed, designed, and fabricated. This is an expanded version of a brief description of the single-polarized MEH design presented in [14]. One of the advantages of the proposed structure in this article is that each subwavelength (∼0.14 λ) unit cell is insensitive to polarization. This article investigates two styles of the proposed MEH, namely, the conventional flat MEH and the flexible 2-D-isotropic as a new classification of MEH. The former style will be compared with the other related published works. However, the flexible 2-D-isotropic MEH is the main goal of this article. A significant reduction in the design process time is achieved using a surrogate model of resonant dipole antenna embedded in the medium [14]. A vital challenge of designing MEH is its impedance matching. We have used a classic approach to tune this device with different

Manuscript received October 14, 2019; revised December 25, 2019; accepted January 31, 2020. *(Corresponding author: Khalil Mafinezhad.)*

Alireza Ghaneizadeh, Abbas Golmakani, and Khalil Mafinezhad are with the Department of Electrical Engineering, Sadjad University of Technology, Mashhad 9188148848, Iran (e-mail: a.ghaneeizadeh@gmail.com; golmakani@sadjad.ac.ir; khmafinezhad@gmail.com).

Mojtaba Joodaki was with the Department of Electrical Engineering, Ferdowsi University of Mashhad, Mashhad 9177948974, Iran. He is now with the Department of Electrical Engineering, Jacobs University of Bremen, 28759 Bremen, Germany (e-mail: joodaki@um.ac.ir; m.joodaki@jacobs-university.de).

Josef Börcsök is with the FG Rechnerarchitektur u. Systemprogrammierung, Universität Kassel, 34121 Kassel, Germany (e-mail: j.boercsoek@uni-kassel.de).

Color versions of one or more of the figures in this article are available online at http://ieeexplore.ieee.org.

Digital Object Identifier 10.1109/TMTT.2020.2982386

loads. Moreover, the EM energy harvesting mechanism is interpreted using a simple equivalent circuit model. To evaluate our design approach, the structure is fabricated using a low-cost PCB technology, and an experimental verification has been demonstrated. The proposed MEH structure can be scaled for other RF bands.

II. Analysis, Modeling, and Design of the MEH

Basically, it is worth mentioning that international organizations (e.g., IEEE, FCC) enforce communication services to get a minimum power level in radio frequency ranges within (semi)urban environments and buildings, for example, LTE, WiFi, and GSM [2]. Generally, these crowded frequency ranges are the vital sources for EM energy harvesting, and thus WiFi (5.85 GHz) as a crowded frequency band [14] was chosen to be the base frequency in our work, which is also used for IoT applications. A popular approach for designing an EM device is the parameter sweeping method using simulation tools guided by engineering experiences and metaheuristic methods [14], [15]. Unfortunately, most of these approaches may be relatively laborious tasks, especially whenever the EM device becomes complex shaped by irregular discontinues and different loads [14]–[16]. Furthermore, it should be mentioned that analytical methods to parametrize meta-structures are hardly available [14], [16]. To overcome these challenges, researchers are aiming to use simple models [14]–[17], and correspondingly, we have proposed a simple model of an extremely ultrathin MEH (EMEH) to predict the resonant frequency of the EMEH [14]. The present model is based on the surrogate model of resonant half-wave dipole antennas [14]. To have a more accurate modeling of the structure, numerical simulation tools [ANSYS HFSS and Advanced Design System (ADS)] are used in this article.

The proposed EMEH consists of copper repeated patches which are linked to the grounded substrate through four loaded metallic vias. The symmetric design offers polarization insensitivity property. The symmetric vertical conducting vias deliver the induced currents to the desired loads. Rogers RO3010 PCB substrate ($\tan(\delta) = 0.0022$ and $\varepsilon_r = 11.2$) as the dielectric insulator is used with a thickness of 0.254 mm.

Fig. 1 illustrates the schematic drawing (with different scales) of the used unit cell. The dielectric which is sandwiched between the bottom and the top metal layers has a deep subwavelength ($\sim$0.004 λ_0) thickness; thus, these metal layers constitute a very strong capacitance. To make an efficient capacitance coupling, the top-layer patches are made with PCB technology etching of the infinitesimally thin slots [18] whose widths (150 μm) are in the order of 0.002 of the wavelength of operation. In practice, the periodicity (P) of these grids in the x- and y-axis is calculated as follows [14]:

$$P = \frac{\lambda_m}{2} = \frac{c}{2f\sqrt{\varepsilon_r}} \tag{1}$$

where λ_m, ε_r, c, and f are the guided wavelength, the permittivity used in the substrate of EMEH, the free-space velocity of light, and the resonance frequency, respectively.

Basically, the real part of average power (time-harmonic) containing power consumption, generation, and losses is

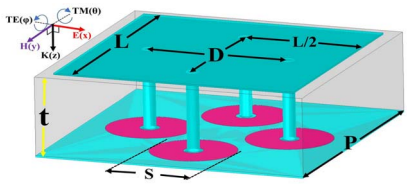

Fig. 1. Schematic 3-D drawing of the proposed EMEH unit cell (P = 7.66 mm, L = 7.51 mm, S = 2.4 mm, D = 4 mm, t = 0.254 mm = 10 mil).

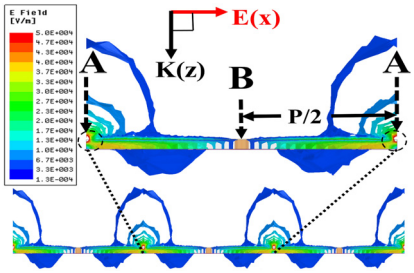

Fig. 2. Full-wave simulation of the electric field distributions at resonance frequency (5.82 GHz) viewed in the x-z plane.

relevant to the imaginary part of permeability (μ) and permittivity (ε) based on Poynting theorem [13]. Because PCB substrate and copper losses are insignificant, the input impedance of the EMEH without loads approaching to free space is almost completely reactive similar to a typical high-impedance surface (HIS) [19]. Traditionally, the metal patches with subwavelength periodicity illuminated with the plane wave have capacitive characteristics acting as dipole type of frequency selective surfaces (FSSs) [23]. To provide a resonant structure in the path of an incident plane wave, these capacitive FSSs are placed on the thin grounded substrate because each thin grounded dielectric has the inductive characteristics [23]. However, the loads have changed the nature of the structure to an energy harvester [19]. The magnitude of the reflection coefficient ($\tilde{A}$) at the interface between free-space impedance (Z_0) and the input impedance of EMEH (Z_{EMEH}) is formulated as [18]

$$|\Gamma| = \sqrt{\frac{(\text{Re}\{Z_{\text{EMEH}}\} - Z_0)^2 (\text{IM}\{Z_{\text{EMEH}}\})^2}{(\text{Re}\{Z_{\text{EMEH}}\} + Z_0)^2 (\text{IM}\{Z_{\text{EMEH}}\})^2}}. \tag{2}$$

The reflection coefficient magnitude of an unloaded EMEH is close to unity. Furthermore, copper grounded substrate reduces the transmission coefficient magnitude of EMEH to nearly zero [18]. Thus, the loads are used to mimic the behavior of $\text{Re}\{Z_{\text{EMEH}}\}$ or compensate the imaginary part of μ and ε of EMEH to realize EM energy harvesting at the resonance frequency.

A. Analysis of EMEH

Fig. 2 depicts the full-wave simulation results of the electric field distribution over the repeated unit cell for a normal incident wave with x-polarization at the resonance frequency.

As it is observed, the electric field is mostly concentrated on the slots that are parallel to the y-axis. Indeed, they strongly couple into the local infinitesimal areas. It is seen that a loose coupling arises in the middle of the cells above the two middle

vias along the y-axis. The distance between the maximum and the minimum of the electric field distributions is $\lambda_m/4$ [see Fig. 2]. Based on the Schelkunoff's equivalence principle, the interactions between the EM incident wave and the EMEH can be explained by the induced currents [20]. In fact, the incident wave can induce both the electric and magnetic dipole moments on the EMEH unit cells required to generate the induced sheet current densities leading to secondary wavefronts to satisfy EMEH's boundary conditions [21]–[23].

For modeling the behavior of the structure to a simple resonant circuit, we consider an electrostatic point-view of Fig. 2.

The electric field can be considered as an induced differential electric potential around the slots, which causes charge distribution to be accumulated close to the edge of cells. The product of voltage (V) and capacitance (C) is equal to the accumulated charges on the EMEH surface ($Q = \mathrm{CV}$) [24]. The fringing electric field within the slots contributes to a fringing capacitance that helps realize MEH over extremely ultrathin substrates [13], [18]. Perfect absorption of the incident wave requires a nonzero thickness (but electrically small) structure to trap both the induced electric and fictitious magnetic currents known as Huygens surfaces [14], [21]–[23]. Conceptually, the proposed EMEH can respond to the time-varying incident plane wave as the charges oscillate and move with the maximum velocity at B and the minimum velocity at A [see Fig. 2]. When the moving charge distribution reaches B, the magnetic flux is at its maximum value, according to Faraday' law. Clearly, all these time-varying currents that pass through a loop consist of the patch, grounded substrate and the loaded via that can be described as an inductance. The time-varying magnetic flux and the currents contribute to create and electromotive force (emf).

To understand why a surrogate model of the resonant dipole antenna can well predict some responses of EMEH to a plane wave incidence, we should pay attention to the near-field analysis presented in Fig. 3. This figure demonstrates the electric and magnetic field distributions of the EMEH illuminated by a normal incident plane wave for different relative phases of 0°, 45°, and 90°. Evidently, the direction of the electric and magnetic fields is orthogonal to each other with different phase of approximately 90° on the surface at any time. This indicates the existence of the reactive power in the near-field region of EMEH and also it should be mentioned that the reactive power is used for balancing the near-field power at each cycle of time-harmonic fields [25]. In its simplest model, the magnitude of the electric and magnetic fields over the unit cell is similar to those of the resonant electric and magnetic dipole antenna, respectively [26], [27]. Accordingly, the impedance and pattern data of dipole antennas may be used to predict the proposed EMEH [28].

B. Input Impedance

Generally, the key factor of any radiator or collector is characterized by its input impedance as an EM gate for reception and radiation within a limited bandwidth [27]. An objective of the EMEH is to determine the ratio of the electric

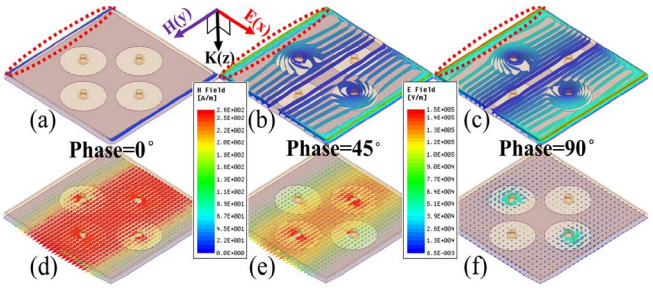

Fig. 3. (a)–(c) Electric and (d)–(f) magnetic field distributions in the unit cell when EMEH is illuminated by a normal incident plane wave (electric field in the x-direction) for different relative phases of 0°, 45°, and 90° at 5.82 GHz.

to magnetic fields (input impedances) at each port's surface for impedance matching. The boundary condition of the surface can be determined by its surface impedance [19]. The EM fields are vectorial quantities [24]. Typically, the transverse magnetic (TM) and transverse electric (TE)-polarized plane wave incidences have a surface wave impedance based on the angle of radiation (θ) as [19], [29]

$$Z_{\mathrm{TM}} = Z_0 \times \cos(\theta) \tag{3}$$

$$Z_{\mathrm{TE}} = Z_0 / \cos(\theta) \tag{4}$$

where Z_0 is the impedance of free space. The efficiency can be increased by impedance matching while it results in the reduction in the half power bandwidth (HPBW) ratio. In other words, there is a tradeoff between impedance matching and HPBW at various θs. Correspondingly, another aspect to be considered for EMEH design is the variation in the surface impedance of the EMEH with respect to the angle of the incident wave [28].

Using the transmission-line model (TL) of resonant dipole antennas, the relationship between the desired impedance load and its location can be obtained [27], [28]. This situation is analogous to an open-circuit TL. In principle, the idea of impedance matching is inspired from the modified folded dipole antenna which is traditionally called "T-match antenna" (see Fig. 4, [28]). Wide-range tuning of terminal resistance is achieved by this classic technique with no strong effect on the resonance frequency, that is, the impedance related to the D value in Fig. 1 [28]. Fig. 5 shows the flowchart of the design process of the proposed EMEH. To obtain an initial approximation of D at "T-match antenna" technique to start the optimization loop in Fig. 5, we can use a simple model of our structure with a dipole antenna (see Figs. 5–13 in [28]). The radiation resistance of this dipole antenna at a point (R_1) may be simply transformed to the radiation resistance at a maximum current point on the antenna (R_0) because a variation in its distribution of sinusoidal current may be related to a change in the feed point position by the following equation [28]:

$$R_1 = \frac{R_0}{\cos^2(\beta x)} \tag{5}$$

where β is the phase constant ($2\pi/\lambda$) and x is the nearest distance from the maximum current point to the terminal of the symmetrical, linear, thin, center-fed antenna. It should

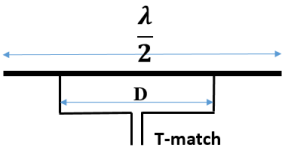

Fig. 4. T-match antenna, from [28].

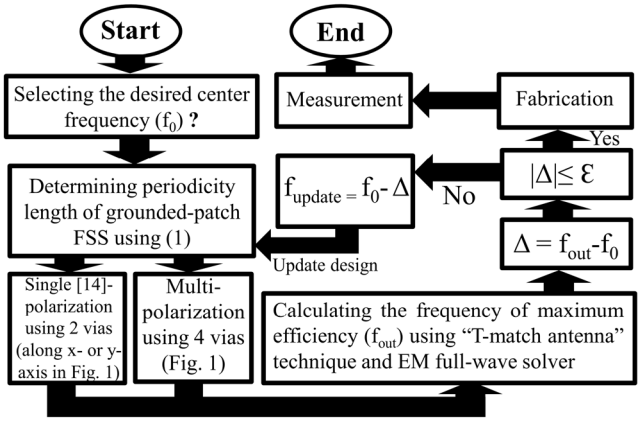

Fig. 5. Flowchart of the design process of the proposed EMEH. Note that the thickness of EMEH (t) and (L/P) as shown in Fig. 1 are about 0.004 λ_0 and 0.98, respectively, during the design process.

be noted that the antenna losses are neglected [28] (see Figs. 5–13 in [28]).

In Fig. 1, S is selected for SMA connector of 2.4 mm. For better demonstration, efficiency versus D variation from 3.4 to 5.2 mm is presented in Fig. 6(a) and (b) for two loads of 35 and 120 Ω, respectively. As shown in Fig. 6(a), for EMEH with a lower impedance load (35 Ω), the efficiency is increased by decreasing D. In contrast, for EMEH with a higher impedance load (120 Ω), the efficiency is improved by increasing D. Therefore, for a lower/higher load impedance, we need a smaller/bigger D for achieving the maximum efficiency. In addition, lowering D leads to a reduction in the resonant frequency of the structure. The reason behind this effect is the longer current path of charge carriers from the edge of the cells. In the circuit point-view, the reduction in D causes a larger inductance (current path), while the capacitance of the whole structure is almost constant [$f = 1/2\pi\ (LC)^{1/2}$]. In "T-match antenna" technique, we have limited freedom to D variation in Fig. 1 which is due to experimental difficulty, the precision of the fabrication process, and also because of the diameter of the SMA connector and the required tolerance. Thus, we could not reduce the D value to less than 4 mm in our structure. Actually, the EMEH as a matching network could not exactly match the impedance of free space ($120\pi\,\Omega$) to load of 50 Ω in normal incidence. That is why perfect absorption is observed at TM 60° instead of TM 0°. This means that EMEH loads match to $60\pi\,\Omega$ according to (3). In spite of all this unwanted mismatching, the efficiency for the normal incident is 87.35%, which is comparable with the other state-of-the-works in Table I.

To demonstrate the physical concept of the energy harvesting process, the current and magnetic field distributions are shown in Fig. 7 for a normal incident wave with different

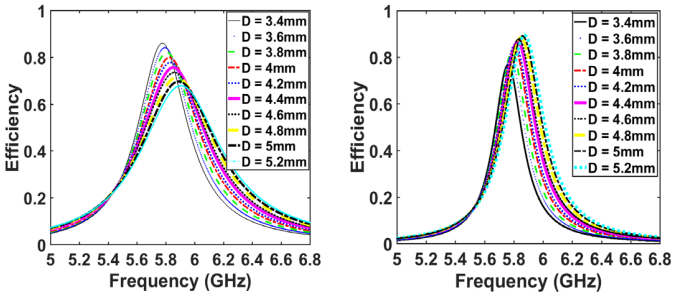

Fig. 6. Simulation result of efficiency versus D variation from 3.4 to 5.2 mm with two tested input impedances (a) 35 and (b) 120 Ω when EMEH is illuminated by a normal incident plane wave (electric field in the x-direction).

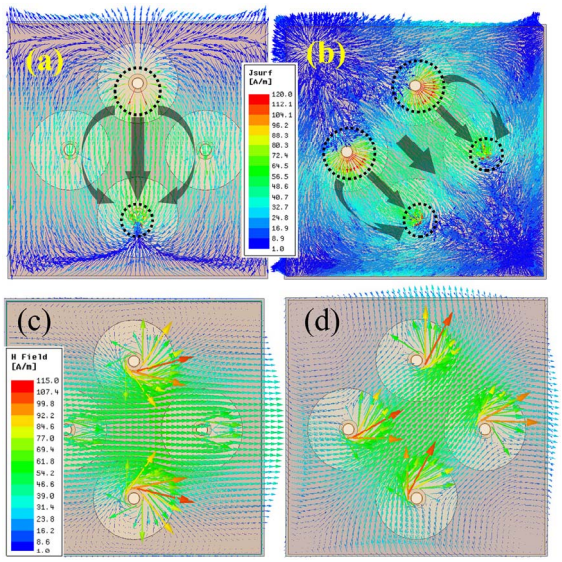

Fig. 7. Results of the current and magnetic field distributions for different relative linear polarization angles at 5.82 GHz (polarization angles of ϕ are from x-axis in the xy plane): (a) current distribution $\phi = 0°$, (b) current distribution $\phi = 45°$, (c) magnetic field $\phi = 0°$, and (d) magnetic field $\phi = 45°$.

polarization angles. Accordingly, it can be seen that the maximum time-changing magnetic flux is passing through the closed path between vias in each unit cell and it can lead to an induced emf.

Fig. 7(a) and (c) designates that polarization of 0° (from the x-axis in the xy plane) can cause contribution of only two metallic vias in the generation of the induced loop current which is similar to our former work with two loaded vias [14]. This is fundamentally true because the magnetic flux direction is perpendicular to the surface enclosed by the loop current path passing through these two vias. Fig. 7(b) and (d) illustrates that the polarization of 45° involves four vias as the magnetic flux causes the induced loop current to be shared between four vias. The symmetric proposed structure is insensitive to polarization of the incident plane wave. However, the value of participation of each couple of vias to the EM energy harvesting depends on the direction of the magnetic flux, based on Faraday's law.

C. Lump Circuit Modeling

As mentioned above, just two induced loaded vias are considered for polarization angle of 0°. To facilitate the

TABLE I

COMPARISON OF THE PROPOSED EMEH WITH PREVIOUSLY PUBLISHED WORKS (NORMAL INCIDENCE $\theta = 0°$)

Ref.	η	P/ λ_0	t (mm)	Style of MEH	FoM
[9]	88%	0.32	0.787	Planar	9.9
[6]	90.7%	0.44	3	Planar	17.3
[31]	92%	0.34	0.79	Planar	19.1
[32]	87%	0.2	1.524	Planar	66.7
[12*]	97.3%	0.16	4	Planar	74.9
[33]	86%	0.12	4.572	Planar	-
[34]	92%	0.15	1.542	Planar	-
[35]	90%	0.13	3	Planar	-
[8]	92%	0.08	2.54	Planar	-
This work	**87.35%**	**0.14**	**0.254**	**Flexible**	**83.1**

*The ratio of thickness to resonance wavelength was published 0.07, but the t to λ_0 ratio computed 0.03 according to the FoM definition.

study of EMEH's cells' behavior toward a normal incident plane wave with polarization of 0°, a simplified equivalent circuit of the proposed unit cell is presented in Fig. 8. For a clearer illustration, Fig. 8(a)–(c) demonstrates the locations of each lump component of Fig. 8(d). Fig. 8(e) compares the responses of the circuit simulator of ADS software and a full-wave simulator of HFSS for calculating the S-parameters. It can be observed that two responses are in good agreement, which indicates that the maximum radiation power is absorbed and divided evenly between the two loads with a minimum reflection. It is worth mentioning that port 1 is specified for the free space with characteristic impedance $Z_0 = 377\ \Omega$ and port 2 is specified for one of the two loaded vias (input impedance of SMA) with characteristic impedance $R_L = 50\ \Omega$. The equivalent lump circuit parameters were estimated by the microstrip line model and then optimized using ADS simulations. The optimized values of the lump parameters are computed as follows: $C_1 = 0.09$ pF, $L_1 = 9.99$ nH, $C_2 = 10$ pF, $L_2 = 9.98$ nH, $C_3 = 0.48$ pF, $L_3 = 9.02$ nH, $C_4 = 1$ pF, $L_4 = 0.36$ nH, $L_5 = 2.96$ nH, $R_1 = 60$ kΩ, $R_2 = 4.25$ kΩ, and $R_3 = 8.5$ kΩ. In addition, the ohmic losses of copper in the microwave regime are ignored, but to consider the dielectric losses, a resistor is added parallel to each lossless capacitor [18].

This kind of modeling with lump circuit components speeds up acquiring the EMEH behavior at a wide range of frequencies without needing the timely full-wave simulation and measurements. In addition, this lump circuit model as a matching circuit helps obtain proper manipulating of its architecture for realizing the desired demands. It should be noted that we have used the full-wave simulation for our final design analysis.

D. Full-Wave Simulation Results

For full-wave simulating of the efficiency, a single cell of the proposed EMEH is located in the *xy* plane. To numerically realize a periodic infinite boundary condition along both the

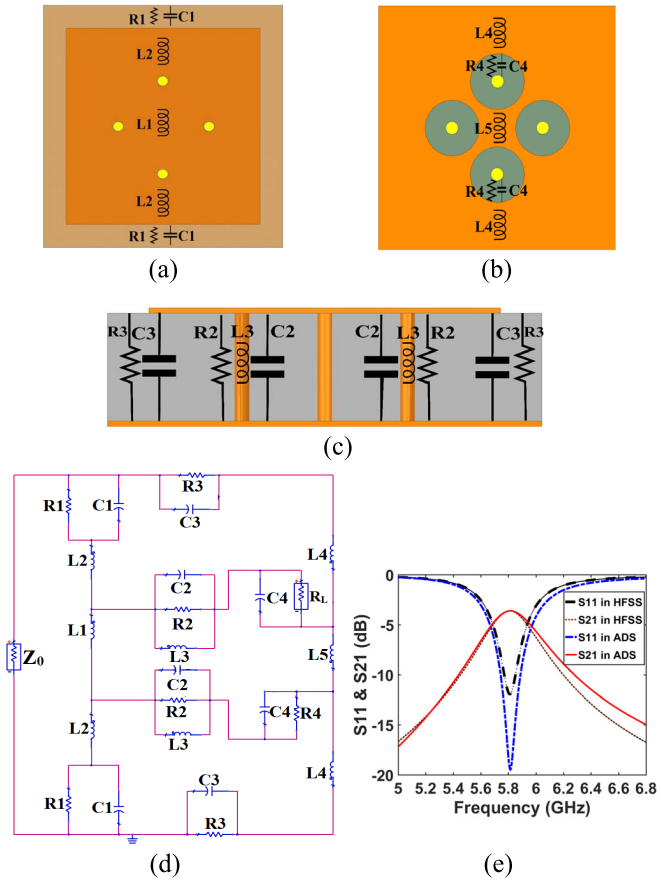

Fig. 8. (a) Top, (b) bottom, and (c) side views of the unit cell illuminated by a normal incident wave with polarization of 0°, (d) a circuit model of the unit cell, and (e) a comparison between the simulation results of HFSS and ADS.

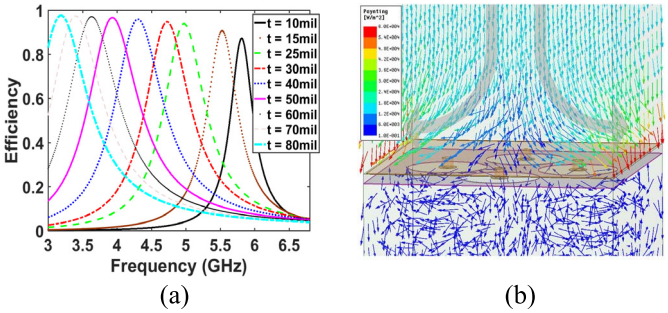

Fig. 9. (a) Efficiency of the structure with different thicknesses of the substrate (t) illuminated by x-polarized normal incident wave and (b) 3-D drawing of real Poynting vector distributions at 5.82 GHz over the unit cell with $t = 10$ mil.

y- and x-directions, we applied the Master and Slave boundary conditions to the lateral walls of the unit cell. To simulate the incident plane wave impinging to the single cell, we considered the Floquet port at the top boundary to excite two orthogonally polarized plane wave modes of TE and TM in HFSS simulator. The efficiency of the EMEH in Figs. 9 and 10 is calculated using its S-parameters which is the sum of the power transferred from the Floquet port to four ports as shown in Fig. 1 which are normalized by the incident wave.

Evidently, a reduction in the thickness of MEH causes some EM limitations which are reviewed in [13]. Reducing the

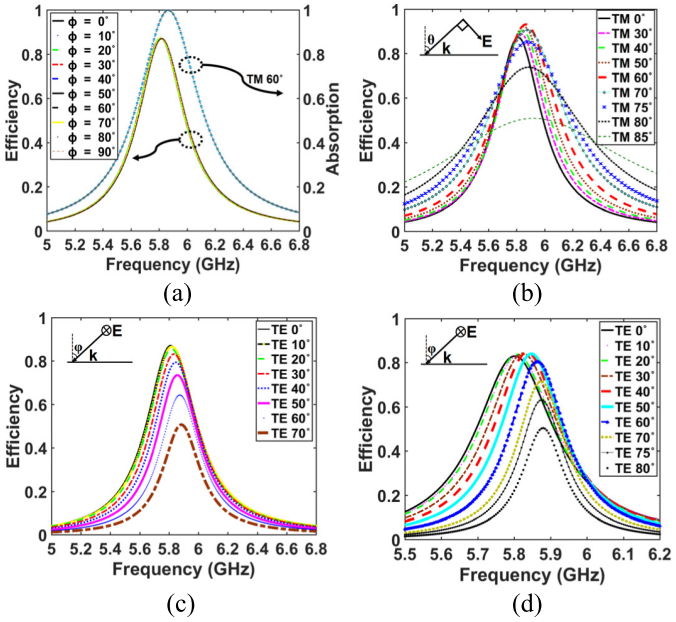

Fig. 10. Simulated efficiency when EMEH is illuminated by (a) normal incident wave with different polarization angles (ϕ), (b) TM-polarized waves with different incidence angles, (c) TE-polarized waves with different incidence angles, and (d) TE-polarized with different incidence angles when EMEH is loaded with 125 Ω. (The right label axis of (a) shows the absorption of EMEH illuminated by TM 60°.)

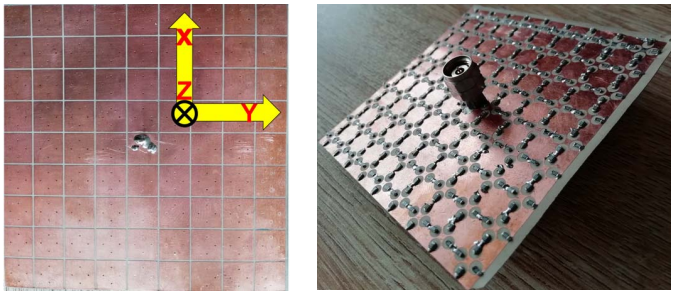

Fig. 11. Fabricated flexible extremely ultrathin EM energy harvester by 9×9 unit cell (a) top and (b) bottom views.

thickness of the EMEH leads to a decrease in the bandwidth and increase in the resonance frequency, and the maximum efficiency of this new type of MEH will be dropped gradually [see Fig. 9(a)]. Fig. 9(b) illustrates how the real Poynting vector redirected itself to the edge of the EMEH cell. The scattered fields from the EMEH are mostly channeling into the lossy environments between the unit cells with minimum reflections at the resonance frequency. This figure obviously indicates that the power of the incidence plane wave is nonuniformly distributed near the surface of the unit cells and most of the radiation wave is converted into guided wave exclusively in the loads.

As a final point, the full-wave simulation shows that the structure is insensitive to the orientation of polarization [see Fig. 10(a)]. For better understanding, it should be said that the incident angle stability of the EMEH is simulated for TM and TE polarizations with different oblique angles in Fig. 10(b) and (c), respectively. The results show that there is an insignificant difference in efficiency from 0° till 75° angle of incidence for TM polarization. The efficiency and HPBW

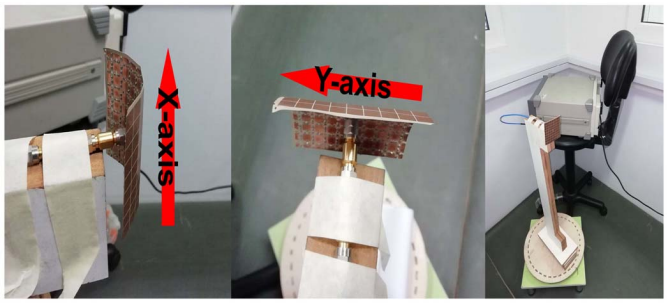

Fig. 12. 3-D-view of (a) curved EMEH bending around the x-axis, (b) curved EMEH bending around the y-axis, and (c) measurement setup.

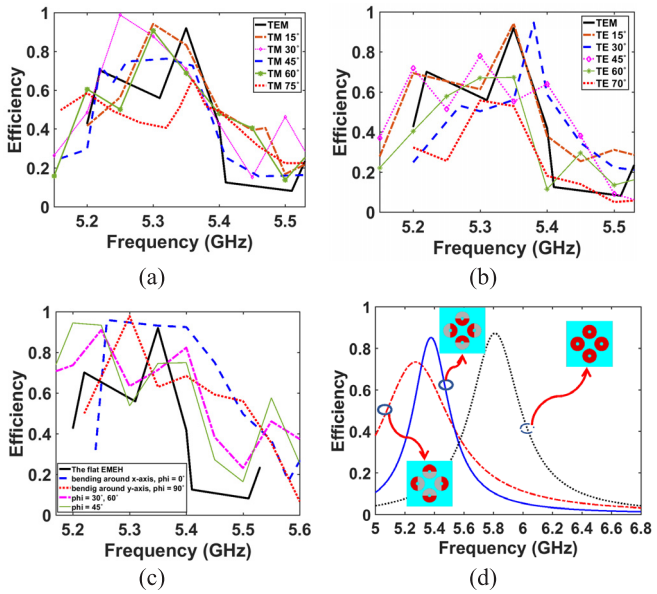

Fig. 13. Measured efficiency when the flat style EMEH is illuminated by (a) normal incident wave (TEM) and TM-polarized waves with different incidence angles, (b) a normal incident wave (TEM) and TE-polarized waves with different incidence angles, and (c) measured efficiency curved EMEH under normal incident wave with different polarization angles (phi). The measured efficiency of the flat style EMEH under normal incident wave (TEM) with polarization of 0° is shown in Fig. 13(a) and (c) for comparing with other results. (d) Full-wave simulation results of efficiency when the flat style EMEH is illuminated by a normal incident wave (TEM) with polarization 0°. [Note that the results of (d) are simulated for the proposed EMEH by just varying the dimensions of lump resistances and their position on the ground.]

of the EMEH are, respectively, 85.37% and 12.86% for 75° oblique angle of TM-polarized incident wave at a resonance frequency of 5.87 GHz.

The absorption of EMEH has been calculated using the formula: $A = 1 - T - R$ [14], in which T, R, and A are the power transmission, reflection coefficient, and the level of absorption, respectively. Perfect absorption is observed at 60° of TM-polarized incident wave in Fig. 10(a). This means that about 6.7% of the incident power is lost in the EMEH and not harvested.

The reasons for angle stability of TM polarization are due to the existence of metallic ground plane [29] and vias in this type of structure [30]. In addition, it is demonstrated that an ultrathin absorber can implicitly restrict the dependence of angular incident on absorption [18]. Furthermore, the dependence of radiation angle on surface wave impedance [29] leads

to an increase in the surface impedance for TE polarization resulting in a lower efficiency compared with TM polarization; see (3) and (4). The full-wave simulation results of the EMEH demonstrated that in the worst case, the maximum efficiency and the resonance frequency at 40° oblique incidence are different by 7.8% and 35 MHz (0.08 of HPBW), respectively, from those of the normal incident wave.

The EMEH structure is studied under a different load of 125 Ω for the TE-polarized incident wave as shown in Fig. 10(d). The results demonstrate that the load values can manipulate the surface impedance of EMEH to match the free-space impedance and improve the efficiency. This indicates that a load larger than 50 Ω is needed for TE polarization, which is in contrast to TM polarization. Therefore, the load impedance should be optimized for the best TM and TE efficiencies. To overcome this tradeoff in designing of flat EMEH, we proposed and fabricated a new flexible structure using symmetric patch FSS. The proposed EMEH can be easily curved in a cylindrical shape to capture EM energy with 2-D-isotropic characteristic with no polarization dependence.

Furthermore, we tried to consider all performance parameters of EMEH in a single formula (6) as a figure-of-merit (FoM) which was introduced in [13]. To this end, Table I demonstrates a fair comparison of our work with other state-of-the-art MEHs converting radiation power to ac power which are reported in the literature so far

$$\text{FoM} = \frac{\text{HPBW} \times \eta \times \cos(\theta)}{t \times P} \times \lambda_0^2 \tag{6}$$

where P, t, λ_0, θ, and η are the length of periodicity, the substrate thickness, the free-space wavelength at the middle frequency of HPBW, the angle of incidence, and the peak of efficiency, respectively.

III. Experimental Results and Discussion

To validate the design concept, the proposed EMEH based on the Rogers 3010 substrate with the thickness of 0.254 mm ($t = 10$ mil) by 9×9 cells is fabricated [see Fig. 11]. A total of 323 SMD resistors are welded to all metallic-vias except one via of the central cell, which is connected to the SMA connector. SMD resistors of 49.9 Ω are placed across the small areas between the via-pad and ground as shown in Fig. 11(b). We measured the fabricated EMEH array at the far-field region of the transmitter horn antenna (distance of 5.2 m). The horn antenna is fed by a Hewlett Packard 83732B signal generator with a power level of 17 dBm. The EMEH is connected to the spectrum analyzer of NS-132 to measure the delivered power to the central cell. The measurement setup is calibrated by considering the connectors, antenna, and cable losses. Due to our symmetrical EMEH structure, we measured the total power of the four loads by rotating the array around the SMA connector in four steps of 90° and accumulating the measured results [6].

From [13], for a fair comparison of the simulation and experimental results, we need to extract an effective area of the central cell (A_f) because of the nonuniform mutual power coupling among the fabricated cells. We obtained an A_f of 3.9 times of the unit-cell physical area (A_p) from our measurements ($A_f = 3.9 \times A_p$). To calculate the harvesting efficiency (η) at the fabricated central cell using the Friis equation, the available incident power (P_{in}) and η are determined as follows [13]:

$$P_{\text{in}} = \frac{P_t \times G_t}{4\pi d^2} \times A_f \tag{7}$$

$$\eta = \frac{P_m}{P_{\text{in}}} \tag{8}$$

where P_m, d, P_t, and G_t are the measurable power delivered to the central cell's loads, the distance between the EMEH and the horn antenna, the radiated power, and the gain of the horn antenna, respectively.

As discussed in [13], to investigate the 2-D-isotropic properties of the MEH (as a small slice of the cylinder), we considered a curved EMEH with a radius of $r = 48$ mm under normal incident wave as shown in Fig. 12(a) and (b). Fig. 12(c) illustrates a part of our measurement setup.

Fig. 13(a) and (b) depicts the efficiency of the flat style EMEH at different oblique incidence angles for TM and TE polarizations, respectively. The direction of the ambient incident plane wave is practically unknown (random). If we consider the central axis of the cylinder as the x-axis, this structure could receive the wave energy in all directions perpendicular to this axis. The experimental results in Fig. 13(c) demonstrate that EMEH efficiency remains nearly unchanged for the curved device under a normal incident wave. Polarization insensitivity of the curved EMEH is shown in Fig. 13(c) and is measured by rotating the curved EMEH around the SMA connector under the normal incident wave.

The discrepancy between the measured and simulated results is mainly due to the infinite number of cells used in our full-wave simulations, while the experimental results are obtained from the EMEH with 81 cells. In fact, the length of the current path on the ground plane is increased because almost all currents have to pass through SMD resistances with the standard SMD size of 0603. The full-wave simulation results of Fig. 13(d) show that the resonance frequency is affected by varying the dimensions of the lump resistances and the position of the resistances on the ground. The simulation results of Fig. 13(d) are for the case of resistance dimensions that are equal to half of the lump port dimension (red areas) in Fig. 1 as shown in Fig. 13(d).

There are also construction errors such as tolerance of SMD resistors, soldering, and connector impact. In addition, the residual interference from the reflection of the measuring equipment in the laboratory adds to the reasons explaining the difference between the experimental and simulation results.

IV. Conclusion

We introduced a new multipolarized, flexible, 2-D-isotropic, and extremely ultrathin ($\sim$0.004 λ_0) MEH. A surrogate model according to the dipole antennas is used for designing its resonance frequency and its impedance matching is done using the "T-match antenna" concept. In addition, an equivalent circuit model of our EMEH unit cell is proposed, and its predicted results are compared with those of full-wave simulation. Our theoretical analyses and design approach are supported

by fabrication and experimental measurements. The measured data have an acceptable agreement with the simulation results. Furthermore, this structure shows a perfect absorption at 60° of TM-polarized incidence. This flexible structure can be used in conformal scenarios for realizing IoT applications such as conformal EM absorbers, sensors, and Huygens radiators.

ACKNOWLEDGMENT

This article is an expanded version from the IEEE MTT-S International Microwave Workshop Series on Advanced Material and Processes 2019, Bochum, Germany, July 16th–18th, 2019.

REFERENCES

[1] M. Shirvanimoghaddam *et al.*, "Towards a green and self-powered Internet of Things using piezoelectric energy harvesting," *IEEE Access*, vol. 7, pp. 94533–94556, 2019.

[2] M. Cansiz, D. Altinel, and G. K. Kurt, "Efficiency in RF energy harvesting systems: A comprehensive review," *Energy*, vol. 174, pp. 292–309, May 2019.

[3] O. M. Ramahi, T. S. Almoneef, M. AlShareef, and M. S. Boybay, "Metamaterial particles for electromagnetic energy harvesting," *Appl. Phys. Lett.*, vol. 101, no. 17, Oct. 2012, Art. no. 173903.

[4] O. M. Ramahi, T. S. Almoneef, M. AlShareef, and M. S. Boybay, "Metamaterial particles for electromagnetic energy harvesting," *Appl. Phys. Lett.*, vol. 101, no. 17, Oct. 2012, Art. no. 173903.

[5] T. S. Almoneef and O. M. Ramahi, "Metamaterial electromagnetic energy harvester with near unity efficiency," *Appl. Phys. Lett.*, vol. 106, no. 15, Apr. 2015, Art. no. 153902.

[6] H.-T. Zhong, X.-X. Yang, X.-T. Song, Z.-Y. Guo, and F. Yu, "Wideband metamaterial array with polarization-independent and wide incident angle for harvesting ambient electromagnetic energy and wireless power transfer," *Appl. Phys. Lett.*, vol. 111, no. 21, Nov. 2017, Art. no. 213902.

[7] H.-T. Zhong, X.-X. Yang, C. Tan, and K. Yu, "Triple-band polarization-insensitive and wide-angle metamaterial array for electromagnetic energy harvesting," *Appl. Phys. Lett.*, vol. 109, no. 25, Dec. 2016, Art. no. 253904.

[8] B. Ghaderi, V. Nayyeri, M. Soleimani, and O. M. Ramahi, "Multi-polarisation electromagnetic energy harvesting with high efficiency," *IET Microw., Antennas Propag.*, vol. 12, no. 15, pp. 2271–2275, Dec. 2018.

[9] F. Yu, X. Yang, H. Zhong, C. Chu, and S. Gao, "Polarization-insensitive wide-angle-reception metasurface with simplified structure for harvesting electromagnetic energy," *Appl. Phys. Lett.*, vol. 113, no. 12, Sep. 2018, Art. no. 123903.

[10] B. Ghaderi, V. Nayyeri, M. Soleimani, and O. M. Ramahi, "Pixelated metasurface for dual-band and multi-polarization electromagnetic energy harvesting," *Sci. Rep.*, vol. 8, p. 13227, Sep. 2018.

[11] X. Zhang, H. Liu, and L. Li, "Tri-band miniaturized wide-angle and polarization-insensitive metasurface for ambient energy harvesting," *Appl. Phys. Lett.*, vol. 111, no. 7, Aug. 2017, Art. no. 071902.

[12] X. Duan, X. Chen, Y. Zhou, L. Zhou, and S. Hao, "Wideband metamaterial electromagnetic energy harvester with high capture efficiency and wide incident angle," *IEEE Antennas Wireless Propag. Lett.*, vol. 17, no. 9, pp. 1617–1621, Sep. 2018.

[13] A. Ghaneizadeh, K. Mafinezhad, and M. Joodaki, "Design and fabrication of a 2D-isotropic flexible ultra-thin metasurface for ambient electromagnetic energy harvesting," *AIP Adv.*, vol. 9, no. 2, Feb. 2019, Art. no. 025304.

[14] A. Ghaneizadeh, M. Joodaki, J. Börcsök, and K. Mafinezhad, "A new extremely ultrathin metasurface energy harvester and its simple modelling based on resonant half-wave dipole antenna," in *IEEE MTT-S Int. Microw. Symp. Dig.*, Bochum, Germany, Jul. 2019, pp. 64–66.

[15] O. M. Ramahi and R. Mittra, "A surface integral equation method for the finite element solution of waveguide discontinuity problems," *IEEE Trans. Microw. Theory Techn.*, vol. 39, no. 3, pp. 604–608, Mar. 1991.

[16] S. Koziel and A. Bekasiewicz, *Multi-objective Design Of Antennas Using Surrogate Models*. London, U.K.: World Sci. Eur., 2017.

[17] X.-X. Liu, Y. Zhao, and A. Alu, "Polarizability tensor retrieval for subwavelength particles of arbitrary shape," *IEEE Trans. Antennas Propag.*, vol. 64, no. 6, pp. 2301–2310, Jun. 2016.

[18] F. Costa, S. Genovesi, A. Monorchio, and G. Manara, "A circuit-based model for the interpretation of perfect metamaterial absorbers," *IEEE Trans. Antennas Propag.*, vol. 61, no. 3, pp. 1201–1209, Mar. 2013.

[19] D. F. Sievenpiper, "High-impedance electromagnetic surfaces," Ph.D. dissertation, Dept. Electr. Eng., Univ. California, Los Angeles, CA, USA, 1999.

[20] C. A. Balanis, *Advanced Engineering Electromagnetics*, 2th ed. Hoboken, NJ, USA: Wiley, 2012.

[21] Y. Ra'di, C. R. Simovski, and S. A. Tretyakov, "Thin perfect absorbers for electromagnetic waves: Theory, design, and realizations," *Phys. Rev. A, Gen. Phys.*, vol. 3, no. 3, pp. 1–37, Mar. 2015.

[22] Y. Ra'di, V. S. Asadchy, and S. A. Tretyakov, "Total absorption of electromagnetic waves in ultimately thin layers," *IEEE Trans. Antennas Propag.*, vol. 61, no. 9, pp. 4606–4614, Sep. 2013.

[23] S. B. Glybovski, S. A. Tretyakov, P. A. Belov, Y. S. Kivshar, and C. R. Smiovski, "Metasurfaces: From microwaves to visible," *Phys. Rep.*, vol. 634, pp. 1–72, May 2016.

[24] D. K. Cheng, *Field and Wave Electromagnetics*. Reading, MA, USA: Addison-Wesley, 1983.

[25] S. M. Mikki, Y. Antar, *New Foundations for Applied Electromagnetics: The Spatial Structure of Electromagnetic Fields*. Norwood, MA, USA: Artech House, 2016.

[26] D.-H. Kwon and D. M. Pozar, "Optimal characteristics of an arbitrary receive antenna," *IEEE Trans. Antennas Propag.*, vol. 57, no. 12, pp. 3720–3727, Dec. 2009.

[27] C. A. Balanis, *Antenna Theory: Analysis and Design*, 3th ed. Hoboken, NJ, USA: Wiley, 2016.

[28] J. D. Kraus, *Antennas*, 2th ed. New York, NY, USA: McGraw-Hill, 1988.

[29] P. T. Bowen, A. Baron, and D. R. Smith, "Theory of patch-antenna metamaterial perfect absorbers," *Phys. Rev. A, Gen. Phys.*, vol. 93, no. 6, pp. 1–8, Jun. 2016.

[30] O. Luukkonen, F. Costa, C. R. Simovski, A. Monorchio, and S. A. Tretyakov, "A thin electromagnetic absorber for wide incidence angles and both polarizations," *IEEE Trans. Antennas Propag.*, vol. 57, no. 10, pp. 3119–3125, Oct. 2009.

[31] B. Alavikia, T. S. Almoneef, and O. M. Ramahi, "Complementary split ring resonator arrays for electromagnetic energy harvesting," *Appl. Phys. Lett.*, vol. 107, no. 3, Jul. 2015, Art. no. 033902.

[32] B. Alavikia, T. S. Almoneef, and O. M. Ramahi, "Wideband resonator arrays for electromagnetic energy harvesting and wireless power transfer," *Appl. Phys. Lett.*, vol. 107, no. 24, Dec. 2015, Art. no. 243902.

[33] P. Xu, S.-Y. Wang, and W. Geyi, "Design of an effective energy receiving adapter for microwave wireless power transmission application," *AIP Adv.*, vol. 6, no. 10, Oct. 2016, Art. no. 105010.

[34] M. El Badawe, T. S. Almoneef, and O. M. Ramahi, "A metasurface for conversion of electromagnetic radiation to DC," *AIP Adv.*, vol. 7, no. 3, Mar. 2017, Art. no. 035112.

[35] X. Zhang, H. Liu, and L. Li, "Electromagnetic power harvester using wide-angle and polarization-insensitive metasurfaces," *Appl. Sci.*, vol. 8, no. 4, p. 497, 2018.